BASIC SCIENCE

Nanomedicine: Nanotechnology, Biology, and Medicine
12 (2016) 2283–2290

Original Article

nanomedjournal.com

Nanometer-grooved topography stimulates trabecular bone regeneration around a concave implant in a rat femoral medulla model

Alexey Klymov, MSc[a], Joost te Riet, PhD[b], Peter Mulder[c], Johannes G.E. Gardeniers, PhD[d], John A. Jansen, DDS, PhD[a], X. Frank Walboomers, PhD[a,*]

[a]*Department of Biomaterials, Radboud University Medical Center, Nijmegen, the Netherlands*
[b]*Department of Tumor Immunology, Radboud Institute for Molecular Life Sciences, Radboud University Medical Center, Nijmegen, the Netherlands*
[c]*Institute for Molecules and Materials, Radboud University Nijmegen, Nijmegen, the Netherlands*
[d]*Mesoscale Chemical Systems Group, MESA+ Institute for Nanotechnology, University of Twente, Enschede, the Netherlands*

Received 9 October 2015; accepted 21 June 2016

Abstract

In the present study, a method was developed to reproduce two nanogrooved patterns (groove width/ridge width/depth: 150/150/50 nm and 200/800/70 nm) into cylindrical epoxy resin implants, which were subsequently coated with 20 nm of titanium. Also, implants with a conventional surface roughness (R_q = 1.6 μm) were produced. After cytocompatibility analysis of the produced surfaces, implants were installed into the femoral condyle of rats for 4 and 8 weeks. The histomorphometrical analysis of bone volume in a 100 μm wide zone close to the implant surface showed that only for the 200/800 grooves the amount of bone increased significantly between 4 and 8 weeks of implantation. In addition, at the late time point only implants with the 200/800 pattern revealed a significantly higher bone volume compared to the rough controls. In conclusion, the 200/800 grooved pattern can positively influence bone volume adjacent to the implant surface, and should be evaluated and optimized in further (pre-)clinical studies.

Key words: Nanotopography; Nanogrooves; Bone regeneration; Rat femoral condyle; Bone implants

Musculoskeletal disorders belong to the most common disability conditions affecting more than 8% of the global population.[1] Annually, more than 50 million incidents occur worldwide of which around 10 million require operative procedures including fracture repair and the placement of metallic reconstructive devices.[2] In addition, about one million dental implants are placed worldwide yearly in edentulous patients.[3] While current survival rates of modern titanium implants reach numbers above 95% during a period of 5 years, the success in elderly and compromised patients is significantly lower.[4–6] Moreover, the chance for implant-failure is steadily increasing with the wearing time.[7,8] As the aging of the Western society continues, the healthcare systems will eventually be faced with the problem of reduced implant success rates. Therefore, next generation implants will need to last over a longer period of time and moreover, considering age related diseases like diabetes and osteoporosis, will need to be adapted to compromised situations. For this purpose, optimizing the interface between the implant and the patients' bone seems a promising strategy.

Especially the positive effects of topography on bone implants have been widely recognized. Nearly all modern implants display some sort of surface roughness, which is usually introduced using common industrially applied implant manufacturing methods (i.e., grit-blasting, acid etching, machining).[9,10] In general, surface topographies are thought to directly influence cell-behavior of bone-forming cells by

This work was supported by a grant from the Dutch government to the Netherlands Institute for Regenerative Medicine (NIRM, Grant No. FES0908). Joost te Riet is supported by the Netherlands Organisation for Scientific Research (NWO) (Veni Grant No. 680-47-421). The atomic force microscope work was supported by NWO Medium Sized Investment (Grant No. NWO-ZonMW 91110007). The authors furthermore thank the RIMLS Microscopic Imaging Center for the use of their facilities.

*Corresponding author at: Department of Biomaterials, Radboud University Medical Center, P.O. Box 9101, 6500 HB Nijmegen, the Netherlands.

E-mail address: Frank.Walboomers@radboudumc.nl (X.F. Walboomers).

http://dx.doi.org/10.1016/j.nano.2016.06.013
1549-9634/

mechanical stimulation and interaction with the intracellular signaling pathways mediated by focal adhesions.[11] However, a disadvantage of roughness is the difficulty of characterization, the identification of relevant features needed to induce certain cell-behavior, and therefore the optimization of these features. An improvement of this situation could be the utilization of strictly defined, organized and ordered topographies.

Multiple *in vitro* studies have shown the potential of ordered topographies to directly interact with bone-forming cells.[12–14] Especially grooves with submicron and nano-dimensions were found to be promising in inducing strong effects on osteogenic differentiation and increased mineral deposition *in vitro*.[15–21] The same studies show that the magnitude of such an influence is directly related to the groove/ridge sizes. However, the translation of knowledge, obtained from these *in vitro* studies, to crucial pre-clinical studies occurs rarely. One study that has evaluated the effects of submicron and nano-sized grooves on bone regeneration *in vivo* was performed by Prodanov et al.[22] For the experiment, nanogrooves with groove widths between 75 nm and 500 nm were introduced into flat titanium discs by nanoimprint lithography, which were then compared to conventional grit-blasted/acid etched surfaces. The implants were installed onto the cortical bone of rabbit tibia and the bone-to-implant contact was evaluated 4 and 8 weeks after implantation. The authors found a significantly higher bone-to-implant contact on 225 nm wide grooves compared to a control surface at the early timepoint. However, as bone–implants are generally not planar and for a major part in contact also with trabecular bone the described experimental setup has only limited clinical relevance.

In order to mimic the clinical situation, the here presented study was aimed to produce cylindrical implants with nanosized topographies featured on the entire surface. The effects of clinically applied rough surfaces (R_q = 1.6 μm) were compared to nanogrooves (groove width/ridge width/depth: 150/150/50 nm and 200/800/70 nm) regarding the bone volume adjacent to the implant surface. The implants were implanted in a rat femoral medulla model,[23] and evaluation of bone regeneration was performed after 4 and 8 weeks by histomorphometry.

Methods

Implant production

Figure 1 shows the manufacturing method for the implants. Two silicon wafers were processed by means of laser interference lithography for the production of two different grooved patterns (groove/ridge; 150/150 nm and 200/800 nm), as described before.[24] For a control surface, a rough pattern was introduced in a titanium plate by grit-blasting. The wafers and the titanium plate were used as master-templates for reproduction of the surface topographies into a thin layer of silicone rubber Polydimethylsiloxane (PDMS; Elastosil RT 601, Wacker-Chemie, München, Germany). Afterward, the replicate was rolled up inside a tubular mold for the final production of cylindrical implants. Implants were then cast using a two-component epoxy resin (Araldite/Aradur; Huntsman Corporation, Salt Lake City, UT), resulting in a final dimension of 2.4 mm Ø × 5 mm. Implants were coated with a 20 nm thick titanium (source purity 99.9%) layer by using a 6 kW supersource electron-beam system (Temescal, Livermore, CA), at a base starting pressure of 2×10^{-5} mBar and an evaporation speed of 250 pm/s. For sterilization the implants were gamma irradiated with a radiation dosage between 25 kGy and 50 kGy (Synergy Health, Ede, the Netherlands).

Implant characterization and quality control

The implants were characterized and quality control was performed by means of atomic force microscopy (AFM), electron microscopy and profilometry. For AFM (Catalyst, Bruker, Santa Barbara, CA, USA), samples were analyzed in tapping mode with 118 μm long silicon cantilevers (NW-AR5T-NCHR, NanoWorldAG, Wetzlar, Germany) with average nominal resonant frequencies of 317 kHz and average nominal spring constants of 30 N/m. These AFM probes have a high aspect ratio (7:1) portion of the tip with a nominal length of >2 μm, nominal radius of curvature of the AFM probe tip less than 10 nm and a half-cone angle of <5°. These probes are able to probe deeply into the grooves with minimal artifacts. The analyzed field was scanned at a rate of 1.0 Hz and 512 scanning lines. Nanoscope Analysis software (version 1.50, Bruker) was used to measure the groove dimensions.

For scanning electron microscopy (SEM) the substrates were sputter-coated with gold and surface topography was examined by a JEOL 6310 SEM (Jeol, Tokyo, Japan) and a Zeiss GeminiSEM 300 (Carl Zeiss, Oberkochen, Germany).

To examine the titanium layer, the substrates were embedded in araldite. After polymerization, ultrathin sections were made and observed by transmission electron microscopy (JEOL JEM-1010).

The roughness R_q of the control implants was assessed with the Universal Surface Tester (UST, INNOWEP GmbH, Würzburg, Germany).

To assess the integrity of the implant surface topography and titanium coating stability after implantation, elemental analysis was carried out using Zeiss GeminiSEM 300 equipped with an energy dispersive X-ray spectrometer (Quantax EDS for SEM, Bruker Nano GmbH, Berlin, Germany). The analysis occurred on implants that were extracted from the femurs of rats at week 4 and 8. The mechanical force resulted in partial separation of bone from the implant. EDS analysis was performed for the distribution of elements of interest (Ca, P, O, Ti) in areas which did or did not feature bone.

Cytocompatibility test

Rat bone marrow cells (rBMCs) were obtained from femurs of 6 week-old male Wistar WU rats according to local ethical approval (RU DEC 2012-317). Femurs were washed three times in α Minimal Essential Medium (αMEM; Gibco, Invitrogen Corp., Paisley, Scotland) containing 0.5 mg/mL gentamycin (Gibco) and 3 mg/mL fungizone (Gibco). The epiphyses were removed and cells were flushed out from the diaphyses using αMEM supplemented with 10% fetal calf serum (FCS; Sigma F7524, Taukirchen, Germany), and penicillin (100 U/mL) and streptomycin (10 μg/mL) (Gibco). One day after incubation,

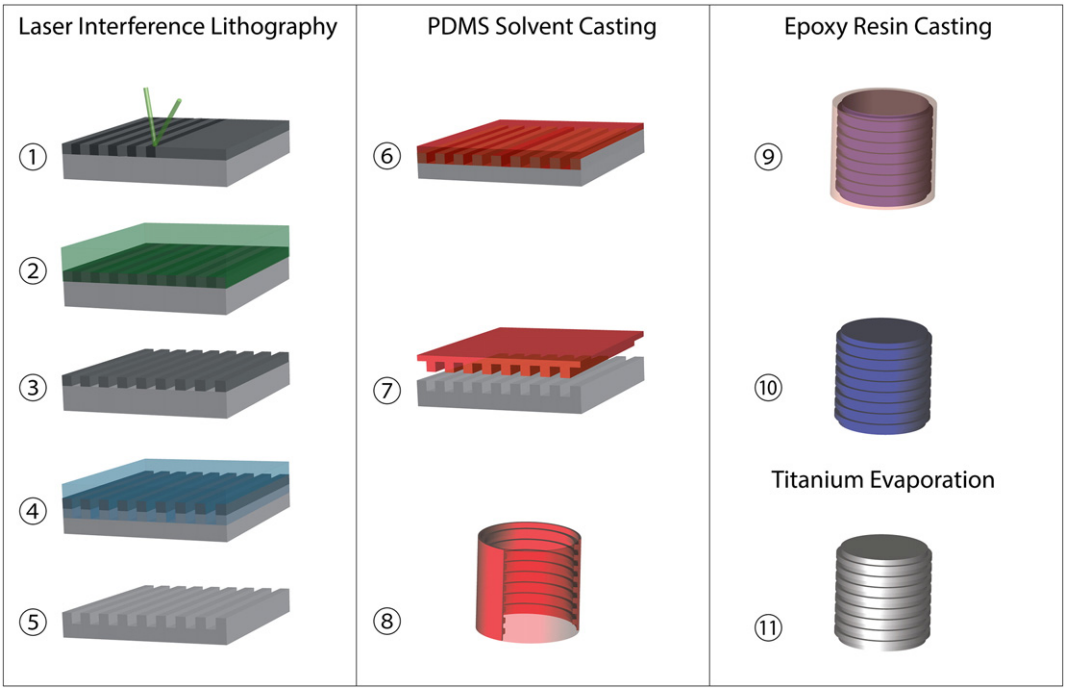

Figure 1. Schematic representation of the nanogrooved implant production. (1) A grooved pattern was written into a photoresist by interference of two laser-beams. (2) The reacted resist was removed. (3) The silicon wafer surface was exposed within the areas that were written into the resist. (4) The exposed silicon was etched to a desired depth. (5) After the remaining resist was removed, the silicon wafer featured the pattern of interest. (6) The wafer was used as a mold for replication of the topography into silicone rubber. (7) After polymerization, the silicone rubber was peeled off from the wafer. (8) The flexible PDMS replicate was introduced into a tube, delivering a curved nanogrooved hollow mold. (9) The mold was filled with an epoxy-resin. (10) After polymerization the rubber was peeled off, leaving the polymeric implant. (11) In the last step a thin layer of titanium was evaporated onto the implant.

non-adherent cells were removed and the medium was refreshed. Cells were allowed to proliferate for 6 days, were collected by trypsinization (trypsin/EDTA; 0.25% w/v trypsin, 0.02% EDTA; Sigma) and seeded onto the implants in a density of 5×10^3 cells/cm^2 in 24-well plates. At day 1 after seeding LIVE/DEAD assay (Molecular Probes, Leiden, the Netherlands) was performed according to the manufacturer's manual. After staining the cells were washed with PBS and evaluated without fixation using a Zeiss fluorescence microscope (Axio Imager Microscope Z1, Carl Zeiss Micro Imaging GmbH, Göttingen, Germany).

Animal experiment

The study was performed according to the guidelines for animal care in the Netherlands and was approved by the Radboud University Nijmegen Medical Center Animal Committee (DEC-2013-121). Male Wistar rats with a pre-surgical weight of approximately 350 g were used. All surgeries were performed under sterile conditions and general anesthesia (Isoflurane). To reduce post-operative pain, Rimadyl (5 mg/kg body weight) was administered subcutaneously before surgery and on days 2 and 3 after surgery. In addition, Temgesic (0.02 mg/kg body weight) was administered immediately after surgery. Bone implantation was performed as described before.[23,25] In short, into the patella–femoral groove a cylindrical hole (diameter: 2.5 mm and depth: 7 mm) was drilled parallel to the long femoral axis. The wider dimension of the drilled cavity was chosen to avoid the destruction of the topography and titanium coating that can occur during a press fit implant insertion. The depth dimension chosen for implantation was to avoid direct implant–growth plate contact. The implants were placed into the trabecular bone of the femoral condyle protruding inside the medullar cavity, and the wound was closed with sutures (Figure 2). The experiments were randomized and blinded. At 4 weeks and 8 weeks the rats were sacrificed by CO_2 suffocation, the femurs were retrieved and used further for fixation and histological staining. In total the following numbers of implants were retrieved and used for histological analysis; Week 4: Rough n = 3, Grooves 150/150 n = 4, Grooves 200/800 n = 4. Week 8: Rough n = 5, Grooves 150/150 n = 4, Grooves 200/800 n = 5.

PMMA embedding, micro-CT and histological evaluation

The explanted femurs were fixed in a 10% formalin solution for a period of 1 week. After fixation the samples were dehydrated in ascending grades of alcohol from 70% to 100%, and embedded in poly(methyl methacrylate) resin. After polymerization, micro-CT was performed on multiple specimens for the visualization of the implant position in bone, using a desktop X-ray micro-tomography system scanner (Skyscan 1072, Kontich, Belgium). 3D reconstruction was performed using CTVox v.2.1 (Skyscan, Kontich, Belgium).

For histology, cross-sections were prepared with a thickness of approximately 10 μm parallel to the long axis of the implant (Figure 3, *A*). A series of at least three sections was made per

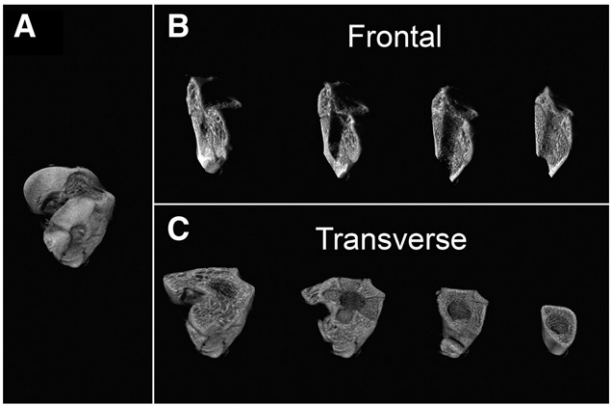

Figure 2. Visualization of implant placement. **(A)** Micro-CT reconstruction of the 200/800 grooves implant in the rat femoral bone, 4 weeks after implantation. **(B)** Digital frontal plane sectioning. **(C)** Digital transverse plane sectioning.

substrate using a modified sawing microtome technique, as described previously by van der Lubbe et al.[26] The PMMA block was oriented with the bone frontal plane parallel to the saw-blade, and a section was made step-by-step until a part of the implant was visible. In case that the section was not in line with the implant the block was slightly adjusted to reduce obliquity of the process, before sections for the analysis were made. The sections were stained with Methylene Blue and Basic Fuchsin. Image acquisition was performed using a slide scanner (Pannoramic SCAN, 3DHISTECH Kft., Budapest, Hungary). Image analysis was performed with Image Pro Plus 6 (Media Cybernetics, Rockville, MD). For the analysis of the bone-volume around the implant, the percentage of positively stained bone in the peri-implant area of 100 μm was quantified (Figure 3, *B-E*). A ratiometric analysis was performed so that obliquity due to non-perfect orientation of bone, would not result in a biased quantification result. Areas that were found to be in contact with cortical bone and/or the growth plate were excluded from further quantification. Only samples with a minimal quantifiable implant/trabecular bone interface of 2 mm were analyzed. Statistical analysis was performed using GraphPad Instat (GraphPad Software, San Diego, CA, USA). Differences in bone volume were calculated using two-way ANOVA with post-hoc Tukey analysis. All measurements were considered independent. Significance was considered at $P < 0.05$. Values are presented as absolute means with standard deviations.

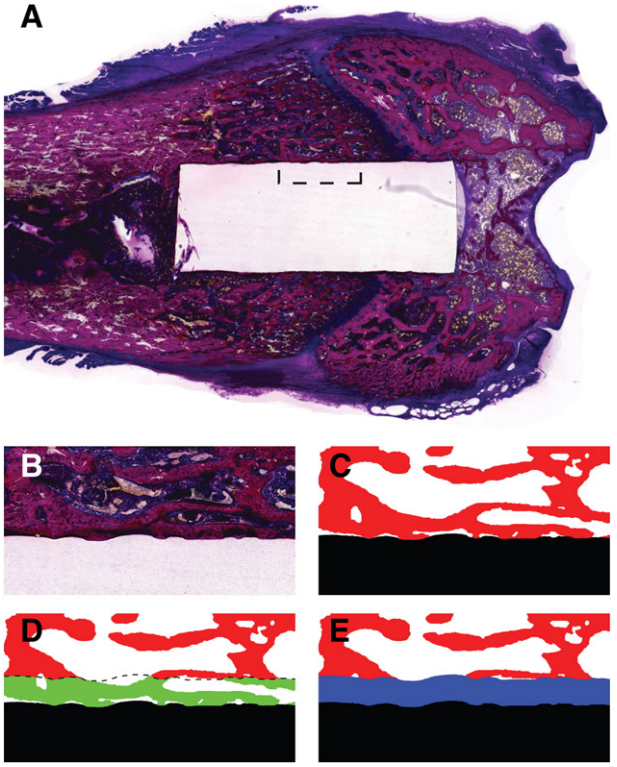

Figure 3. Quantification of bone volume around the implant. **(A)**Micrograph showing a typical histological staining with methylene blue and basic fuchsine. The polymeric implant appears transparent under the light microscope. Areas of the implant that were in contact with the growth plate, or cortical bone were excluded from quantification. The square shows an example of the area that can be used for analysis (magnified in **B**), which is explained in **(B-E)**. **(C)** First bone and implant were reconstructed as monochromatic abstract areas. **(D)** In the second step a mask was made from the implant, and was moved at a distance of 100 μm from the implant surface into the peri-implant area. Inside of the so produced area of interest the bone-positive area (green) was quantified. **(E)** The measured bone area was related to the total area of interest (blue).

Results

Implant quality control

Since the surface topography caused breaking of the reflecting light, implants with a poorly transferred surface topography could immediately be recognized by visual inspection, and were removed (Figure S1). Further inspection by scanning electron micrographs revealed an excellent reproduction quality of the rough and grooved surfaces (Figure 4, *A-C*). Transmission electron microscopy confirmed a continuous thin titanium layer of approximately 20 nm in thickness on the surface of the implants (Figure 4, *D*). While gamma irradiation had no influence on surface topography, a change of the material color was observed from white transparent to yellow transparent. Figure 4, *E-G* shows the atomic force microscope reconstruction of the three titanium coated surfaces. The topographical feature sizes as measured by AFM and UST are reported in Table 1.

The stability of the topography and titanium coating was determined on implants that were explanted after 4 and 8 weeks. Figure 5 shows an area of a 4 weeks implanted 200/800 grooves implant, at which a fracture of the newly formed bone was introduced by explantation forces. No changes to the integrity of the underlying topography were found. EDS analysis confirmed the presence of titanium underneath the bone, as well as on the area where bone was removed (data not shown).

In vitro cell viability

Figure S2 shows the LIVE/DEAD staining of cells cultured for 24 h on the implants. All topographies showed abundant

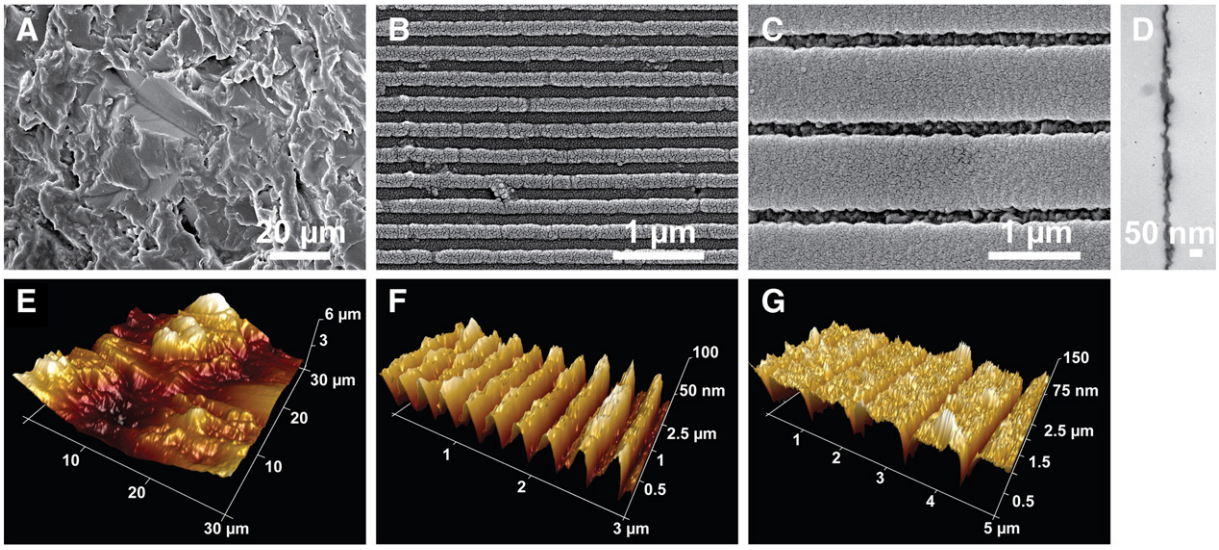

Figure 4. Characterization and quality control of the produced implants. Scanning electron micrographs of **(A)** rough, **(B)** 150/150, and **(C)** 200/800 grooved implants. **(D)** The transmission electron micrograph analysis showed the thin titanium layer on the surface to be approximately 20 nm in thickness. Atomic force microscopy was utilized to characterize the surface feature characteristics of **(E)** rough, **(F)** 150/150, and **(G)** 200/800 grooved implant surfaces.

green calcein-AM and a limited propidium iodide staining. This indicates that all implants can be considered cytocompatible.

General observations animal study

No visible complications could be observed after surgery concerning animal health or behavior. Wound closing occurred without complications. Also no signs of severe inflammation or other adverse tissue reactions were seen. For the histomorphometry between 3 and 5 individual implants per type and time point were evaluated.

Histological and histomorphometrical evaluation

Histological analysis confirmed that the implants were surrounded by trabecular bone. In between the voids of the bone trabeculae bone marrow was present. All implants were found to be intact. The trabecular bone was in direct contact with the implant surface without the presence of an intervening fibrous tissue layer. Subjectively, no major differences were seen between the various implant surfaces. During implantation time (4 vs. 8 weeks), the amount of bone at the implant surface appeared to increase (Figure 6).

Figure 7 shows the results from the quantification of the bone volume at a distance of 100 µm on the peri-implant area. The measured mean bone volume was found to be statistically equal between the various implant surfaces after 4 weeks of implantation, i.e.39% (SD = 11) for the rough, 44% (SD = 10) for the 150 nm grooved patterned and 47% (SD = 12) for the 200/800 grooved surfaces. The histomorphometric evaluation confirmed that a significantly higher bone content was present after 8 weeks (44%; SD = 11) compared to 4 weeks (57%; SD = 13) (pooled data, $P = 0.0006$). Further analysis of the separate data revealed that only for the 200/800 grooved pattern the increase in bone between 4 weeks (47%; SD = 12) and 8 weeks (65%; SD = 7) was significant. In addition, comparison of the 8 week data showed the presence of a significantly higher bone volume around the 200/800 surface (65%; SD = 7), compared to the rough control (49%; SD = 15).

Discussion

While modern clinically available implants still mostly feature low-tech rough surfaces, research evidences the potential of organized nanogrooves to outperform random roughness regarding stimulation of bone-regeneration relevant cell-behavior. However, the limitations of introducing nanotopographies into complex titanium surfaces, such as used in implantology (e.g., circular implants), make production of samples for pre-clinical evaluation rather difficult. In the present study, we used an epoxy resin that was polymerized in a circular nano-patterned mold, resulting in a round-shaped implant. The implants were coated with a thin titanium layer, and were evaluated for their potential to influence the bone-volume at the implant-surface in a rat-femoral medulla model. We found that one of the nanogrooved implants was able to outperform rough implants regarding the quantified trabecular bone volume around the implants.

Considering our experimental setup, several remarks can be made. In general, the described production method was highly reliable and resulted in implants of uniform size and shape. The used resin for the production of implants has excellent reproductive properties and probably can be used for the replication of structures that are smaller than the ones described here. However, Araldite implants are not clinically relevant, as this resin is not used for clinical applications as bone implants. Therefore, Araldite implants were coated with a thin titanium layer. It should be considered that the effects of changes in the pH and temperature as the result of the surgery and inflammation after implantation might induce a change to the implant-surface.

Table 1
Characterization of titanium coated bone implants.

Topography	R_q	Groove width	Ridge width	Groove depth
Rough	1.6 ± 0.1 μm			
150/150		150 ± 5 nm	152 ± 2 nm	47 ± 8.3 nm
200/800		205 ± 32 nm	798 ± 6 nm	67.7 ± 3.5 nm

Especially the stability of the coating is of high importance for our model, as also the material characteristics can influence the final outcome of bone regeneration. The SEM and EDS analysis confirmed that under the here utilized conditions and methods, the topography and coatings were maintained within a period of 8 weeks. The coatings even remained on the surface of the implants after the surrounding bone was mechanically pushed away.

As stated above, in the current study the implants were made out of epoxy with a titanium coating, rather than bulk titanium. Similar epoxy was applied in many cell–surface interaction studies, as it is an excellent material for reproduction of complex surface topographies.[27] Also the coating of epoxy with a thin layer of titanium was intensively studied, and was found compatible in various *in vitro* and *in vivo* setups.[27–31] High cytocompatibility of the finally produced material was also confirmed in the current study by the DEAD/ALIVE assay. Moreover, in order to study biocompatibility implants were also brought in direct contact with soft tissues, by implanting them into subcutaneous pockets (data not shown). After 4 weeks of implantation, all implants were found covered with a fibrous capsule with a thickness of approximately 50 μm. No signs of chronic inflammation were found in histologically stained sections. The findings suggest excellent soft tissue biocompatibility of the topographies and the polymeric/titanium material.

While clinical implants are mostly placed using the standard undersized technique (i.e., the diameter of the drilled cavity is slightly smaller compared to the implant diameter), in the current study we were placing the implants in a wider cavity to avoid destruction of the topography and coating by the extremely dense cortex. Moreover, a 2 mm deeper cavity was produced with respect to the implant size. This was performed to shift the implant past the growth plate and allow for the larger part of the implant to be in direct contact with trabecular bone. The immediate bleeding that was seen in all rats would clot within minutes thereby stabilizing the implant in the deeper part of the femur. During histology no loosening or displacement of the implants was observed. However, such variations of the implantation to the clinically utilized protocols might eventually induce a different bone-response. Having an entirely titanium made implant will allow the application of the regular technique, with reduced chances of damaging the fine surface features. It should also be considered that eventually the topographies have to be manufactured on surfaces of implants that are designed for specific treatments. For example for dental applications screw-type implants are usually used, as to date they have proven to provide an optimal implant fixation. Recently the laser-shock nanoimprinting method was presented that might allow the introduction of ordered nano-topographies directly into metals.[32] Utilizing this technique for the production of patterned implants made from bulk titanium in the form of conventional implants, would allow a setup more comparable to the clinical situation for future studies. This would also avoid the possibility of delamination of the titanium coating, although no evidence of such an event was found in the current study.

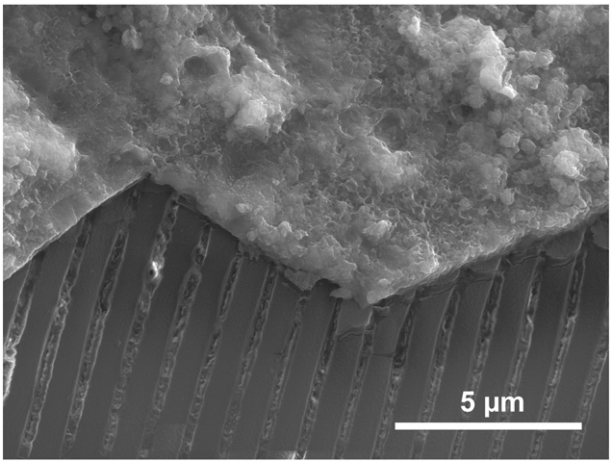

Figure 5. Scanning electron micrograph of an implant after 4 weeks *in vivo*. The fracture of bone was introduced by pushing forces during the retrieval of the implant from the femur. No changes to the integrity of the topography underneath the bone layer were found.

Having solid titanium would also have been beneficial during histomorphometric analysis. Due to the transparent nature of both the epoxy and the embedding resin, the exact border of the implant was often challenging to define exactly. This made it difficult to assess the bone–implant interaction by quantification of the bone-to-implant contact (BIC), i.e., by measuring a single line of contact between the implant and the bone tissue. Thus, the quantification of the bone volume inside a peri-implant area was performed. Earlier studies have measured bone volume at distances of up to 500 μm. However, due to the proximity of the cortex to the medulla region, it is was impossible to measure the trabecular bone volume in distant areas, without including the cortical bone. Thus, a distance of 100 μm was chosen for the current analysis. For future experiments it should be noted that when using the medulla model utilized here, a shorter or smaller diameter implant size should be considered to avoid possible cortical osteoconduction artifacts. Eventually, a monocortical model (e.g., condyle, jaw) could be utilized.

Still, the current investigation proved that the bone volume around bone implants can be manipulated and bone formation around the implant can even be increased by the utilization of a predefined nano-size topography. Histomorphometry showed a significantly higher bone volume around the 200/800 grooved implants, compared to the rough controls. Moreover, the increased bone volume around the implants was significantly higher only for the 200 nm grooved pattern at a comparison between 4 and 8 weeks. In the following steps, it should be elucidated how and to which extent the different topographical features contribute to the observed outcome. One possibility is the increase of the total area on the implant surface, which becomes available for local mineralization. However, the 150/

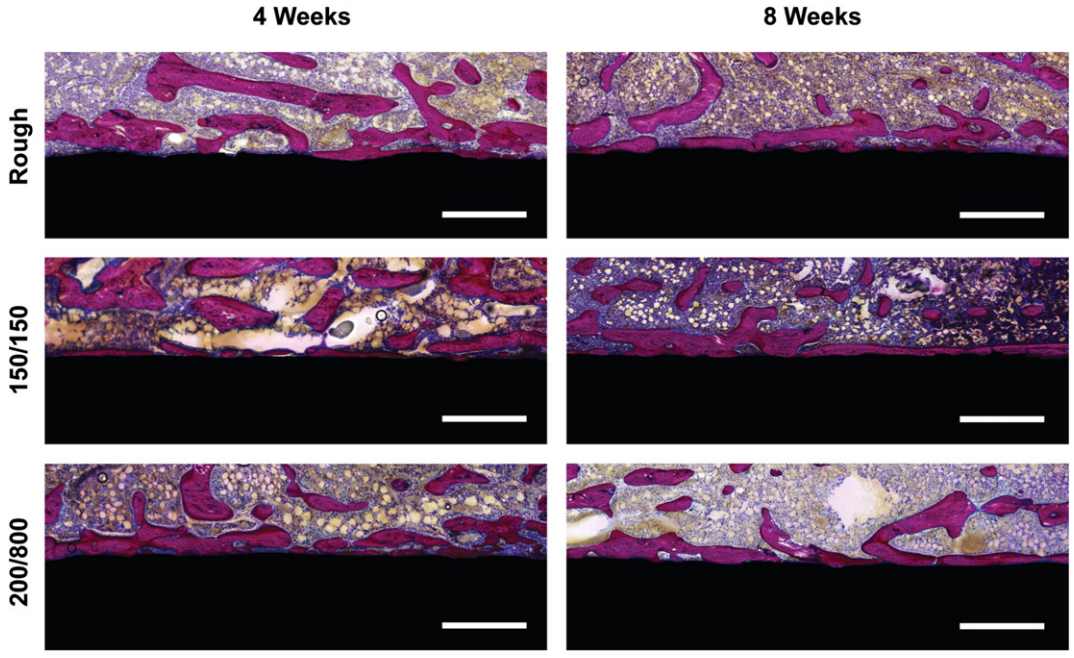

Figure 6. Trabecular bone response to implants 4 and 8 weeks after implantation. Methylene blue and basic fuchsine staining showed in general trabecular bone making direct contact with the implant surfaces and an overall increase in total bone volume around the implants between 4 and 8 weeks (Implants are blacked out). The scale bar represents a distance of 500 μm.

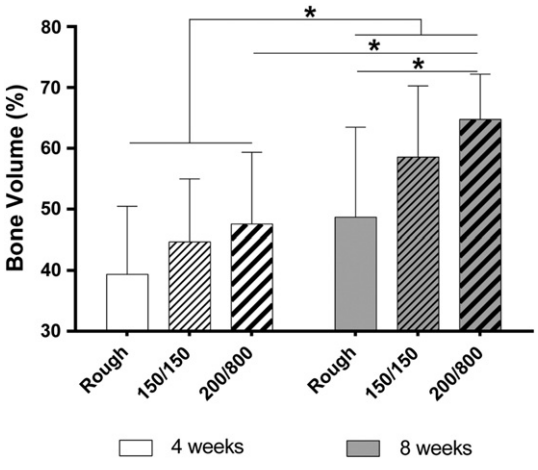

Figure 7. Representation of the obtained trabecular bone-positive area, in the peri-implant area of 100 μm. In general the bone volume around the implant increased between 4 and 8 weeks. A significant difference between grooves and the control rough surface was only observed for the 200/800 pattern at week 8. Moreover, the 200/800 pattern is the only one significantly increasing the bone-positive area between week 4 and week 8.

150 grooves pattern increases the total area by approximately 25%, while the 200/800 grooves increase the surface area only by approximately 12%. Since cells are known to interact mainly with the ridge, when cultured on nanosized grooved patterns,[24,33] the found difference in bone volume could be induced by the differences in the ridge area. The 5.3 times larger ridge area of the 200/800 grooved surfaces compared to the 150/150 grooved surfaces would confirm such a hypothesis. However, the previous *in vivo* study by Prodanov et al. showed that bone-regeneration is dependent on the groove widths, rather than ridge width.[22] The authors report that from the tested groove widths between 75 nm and 500 nm, only the 225 nm wide grooves could induce stronger cortical bone formation at the implant surface. However, contrary to our study the ridge width was 75 nm, while in our experiment the ridge was approximately 800 nm. It has been reported that special disaggregation of focal adhesions inside of cells will define cell behavior, such as cell spreading on a surface.[34] Cell spreading and shape on the other hand are known to influence the differentiation fate of stem cells.[35,36] Although not contributing to the cell-surface adhesion, grooves might indirectly define cell behavior by spatially separating the focal adhesion formations and thereby also the resulting intracellular processes.

Our findings suggest that grooves with widths of about 200 nm have the potential to increase cortical and trabecular bone at the implant–bone interface. However, additional studies are necessary to further evaluate and potentially optimize the manner in which patterns influence bone formation. For example the influence of the ridge dimension should be addressed in more detail in future experiments. Moreover, the influence of patterns should be tested in models that can combine cortical and trabecular bone evaluation, as they might be influenced differently by the same topography.

Appendix A. Supplementary data

Supplementary data to this article can be found online at http://dx.doi.org/10.1016/j.nano.2016.06.013.

References

1. Vos T, Flaxman AD, Naghavi M, Lozano R, Michaud C, Ezzati M, et al. Years lived with disability (YLDs) for 1160 sequelae of 289 diseases and injuries 1990–2010: a systematic analysis for the Global Burden of Disease Study 2010. *Lancet* 2012;**380**:2163-96.
2. *The Orthopaedic Industry Annual Report*. Orthoworld Inc.; 2014
3. Pye AD, Lockhart DE, Dawson MP, Murray CA, Smith AJ. A review of dental implants and infection. *J Hosp Infect* 2009;**72**:104-10.
4. Jung RE, Pjetursson BE, Glauser R, Zembic A, Zwahlen M, Lang NP. A systematic review of the 5-year survival and complication rates of implant-supported single crowns. *Clin Oral Implants Res* 2008;**19**: 119-30.
5. Diz P, Scully C, Sanz M. Dental implants in the medically compromised patient. *J Dent* 2013;**41**:195-206.
6. Total hip replacement and resurfacing arthroplasty for end-stage arthritis of the hip. *NICE Technology Appraisal Guidance*; 2014.
7. Pjetursson BE, Thoma D, Jung R, Zwahlen M, Zembic A. A systematic review of the survival and complication rates of implant-supported fixed dental prostheses (FDPs) after a mean observation period of at least 5 years. *Clin Oral Implants Res* 2012;**23**(Suppl 6):22-38.
8. Bozini T, Petridis H, Garefis K, Garefis P. A meta-analysis of prosthodontic complication rates of implant-supported fixed dental prostheses in edentulous patients after an observation period of at least 5 years. *Oral Maxillofac Implants* 2011;**26**:304-18.
9. Liu R, Lei T, Dusevich V, Yao X, Liu Y, Walker MP, et al. Surface characteristics and cell adhesion: a comparative study of four commercial dental implants. *J Prosthodont* 2013;**22**:641-51.
10. Svanborg LM, Andersson M, Wennerberg A. Surface characterization of commercial oral implants on the nanometer level. *Appl Biomater* 2010; **92**:462-9.
11. Dalby MJ. Cellular response to low adhesion nanotopographies. *Nanomedicine* 2007;**2**:373-81.
12. Klymov A, Prodanov L, Lamers E, Jansen JA, Walboomers XF. Understanding the role of nano-topography on the surface of a bone–implant. *Biomater Sci UK* 2013;**1**:135-51.
13. Lovmand J, Justesen J, Foss M, Lauridsen RH, Lovmand M, Modin C, et al. The use of combinatorial topographical libraries for the screening of enhanced osteogenic expression and mineralization. *Biomaterials* 2009;**30**: 2015-22.
14. de Peppo GM, Agheli H, Karlsson C, Ekstrom K, Brisby H, Lenneras M, et al. Osteogenic response of human mesenchymal stem cells to well-defined nanoscale topography *in vitro*. *Nanomedicine* 2014;**9**: 2499-515.
15. Wittenbrink I, Hausmann A, Schickle K, Lauria I, Davtalab R, Foss M, et al. Low-aspect ratio nanopatterns on bioinert alumina influence the response and morphology of osteoblast-like cells. *Biomaterials* 2015;**62**:58-65.
16. Kim J, Kim HN, Lim KT, Kim Y, Seonwoo H, Park SH, et al. Designing nanotopographical density of extracellular matrix for controlled morphology and function of human mesenchymal stem cells. *Sci Rep* 2013;**3**:3552.
17. Kim J, Kim HN, Lim KT, Kim Y, Pandey S, Garg P, et al. Synergistic effects of nanotopography and co-culture with endothelial cells on osteogenesis of mesenchymal stem cells. *Biomaterials* 2013;**34**:7257-68.
18. You MH, Kwak MK, Kim DH, Kim K, Levchenko A, Kim DY, et al. Synergistically enhanced osteogenic differentiation of human mesenchymal stem cells by culture on nanostructured surfaces with induction media. *Biomacromolecules* 2010;**11**:1856-62.
19. Wang PY, Li WT, Yu JS, Tsai WB. Modulation of osteogenic, adipogenic and myogenic differentiation of mesenchymal stem cells by submicron grooved topography. *J Mater Sci Mater Med* 2012;**23**: 3015-28.
20. Watari S, Hayashi K, Wood JA, Russell P, Nealey PF, Murphy CJ, et al. Modulation of osteogenic differentiation in hMSCs cells by submicron topographically-patterned ridges and grooves. *Biomaterials* 2012;**33**: 128-36.
21. Klymov A, Song J, Cai X, Te Riet J, Leeuwenburgh S, Jansen JA, et al. Increased acellular and cellular surface mineralization induced by nanogrooves in combination with a calcium-phosphate coating. *Acta Biomater* 2016;**31**:368-77.
22. Prodanov L, Lamers E, Domanski M, Luttge R, Jansen JA, Walboomers XF. The effect of nanometric surface texture on bone contact to titanium implants in rabbit tibia. *Biomaterials* 2013;**34**:2920-7.
23. Alghamdi HS, Bosco R, van den Beucken JJJP, Walboomers XF, Jansen JA. Osteogenicity of titanium implants coated with calcium phosphate or collagen type-I in osteoporotic rats. *Biomaterials* 2013;**34**:3747-57.
24. Lamers E, Walboomers XF, Domanski M, te Riet J, van Delft FC, Luttge R, et al. The influence of nanoscale grooved substrates on osteoblast behavior and extracellular matrix deposition. *Biomaterials* 2010;**31**: 3307-16.
25. Alghamdi HS, Cuijpers VMJI, Wolke JGC, van den Beucken JJJP, Jansen JA. Calcium-phosphate-coated oral implants promote osseointegration in osteoporosis. *J Dent Res* 2013;**92**:982-8.
26. van der Lubbe HB, Klein CP, de Groot K. A simple method for preparing thin (10 microM) histological sections of undecalcified plastic embedded bone with implants. *Stain Technol* 1988;**63**:171-6.
27. Chehroudi B, Gould TR, Brunette DM. Effects of a grooved epoxy substratum on epithelial-cell behavior *in vitro* and *in vivo*. *J Biomed Mater Res* 1988;**22**:459-73.
28. Schuler M, Kunzler TP, de Wild M, Sprecher CM, Trentin D, Brunette DM, et al. Fabrication of TiO_2-coated epoxy replicas with identical dual-type surface topographies used in cell culture assays. *J Biomed Mater Res A* 2009;**88A**:12-22.
29. Wieland M, Chehroudi B, Textor M, Brunette DM. Use of Ti-coated replicas to investigate the effects on fibroblast shape of surfaces with varying roughness and constant chemical composition. *J Biomed Mater Res* 2002;**60**:434-44.
30. Chehroudi B, Gould TR, Brunette DM. A light and electron microscopic study of the effects of surface topography on the behavior of cells attached to titanium-coated percutaneous implants. *J Biomed Mater Res* 1991;**25**:387-405.
31. Chehroudi B, Ghrebi S, Murakami H, Waterfield JD, Owen G, Brunette DM. Bone formation on rough, but not polished, subcutaneously implanted Ti surfaces is preceded by macrophage accumulation. *J Biomed Mater Res A* 2010;**93**:724-37.
32. Gao H, Hu YW, Xuan Y, Li J, Yang YL, Martinez RV, et al. Large-scale nanoshaping of ultrasmooth 3D crystalline metallic structures. *Science* 2014;**346**:1352-6.
33. Lamers E, van Horssen R, te Riet J, van Delft FCMJM, Luttge R, Walboomers XF, et al. The influence of nanoscale topographical cues on initial osteoblast morphology and migration. *Eur Cell Mater* 2010;**20**: 329-43.
34. Cavalcanti-Adam EA, Micoulet A, Blummel J, Auernheimer J, Kessler H, Spatz JP. Lateral spacing of integrin ligands influences cell spreading and focal adhesion assembly. *Cell Biol* 2006;**85**:219-24.
35. Wang X, Song W, Kawazoe N, Chen G. Influence of cell protrusion and spreading on adipogenic differentiation of mesenchymal stem cells on micropatterned surfaces. *Soft Matter* 2013;**9**:4160-6.
36. Kilian KA, Bugarija B, Lahn BT, Mrksich M. Geometric cues for directing the differentiation of mesenchymal stem cells. *S A* 2010;**107**: 4872-7.